# Deriving Nighttime Light Metrics for Disaster Assessment Towards Area Prioritisation and Tracking

Leal L.A.B.[1*], Carpio J.A.M.F.[2], Getigan N.M.B.[2], Rubio A.M.C.[2], Paet L.B.B.[1] and Reyes R.C.[1]

[1]*Philippine Space Agency, Metro Manila, Philippines*

[2]*Department of Physics, Ateneo de Manila University, Metro Manila, Philippines*

*lois.leal@philsa.gov.ph

***Abstract*** *Disasters generate widespread damage and displacement, requiring scalable methods to track impact and recovery over time. This study introduces a unified nighttime lights (NTL) framework that integrates percent-based and difference-based metrics with a temporal point of interest approach for continuous disaster assessment and area prioritisation. Using 12 years of NASA VIIRS VNP46A3 data, we analyse 281 barangays in Eastern Visayas, Philippines, affected by Super Typhoon Yolanda (Haiyan) in 2013, capturing the full arc from impact to recovery. Results show severe losses (up to −148.3 nW/cm²/sr, −85.11%) and recovery trajectories extending over 11.5 years, with 57 barangays still below pre-disaster levels as of May 2025. The framework reveals long-term dynamics including displacement, resettlement, and infrastructure-driven gains, aligning with high-resolution imagery and reports. Beyond Haiyan, this approach provides a generalisable, data-driven system for disaster tracking, supporting evidence-based recovery planning and scalable prioritisation across Asia and beyond.*

*Keywords: area prioritisation, disaster assessment, disaster metrics, nighttime lights, tracking*

## 1 Introduction

Nighttime lights (NTL) data are increasingly being studied and used by humanitarian organisations to assess disaster impact and recovery (Zhao et al., 2019; Levin et al., 2020; Group on Earth Observations [GEO], 2023). Decision-makers, however, require systems that can efficiently track disaster effects as new data emerge and prioritise areas most in need of support.

This study introduces a unified framework for disaster monitoring that integrates percent- and difference-based NTL metrics with a temporal point of interest (POI) approach and an area prioritisation mechanism. The framework is demonstrated using the NASA VIIRS VNP46A3 Lunar Gap-Filled BRDF-corrected NTL product for Super Typhoon (STY) Yolanda (Haiyan) in 2013. A 12-year analysis across 281 barangays in Tacloban City, Municipality of Palo, and Ormoc City captures the full arc from impact to recovery,

including patterns of displacement and resettlement.

The paper is organised as follows: Section 2 reviews related studies; Section 3 describes the study areas and methodology; Section 4 presents results, including metrics, tracking, area prioritisation, and limitations; Section 5 concludes.

## 2 Literature Review

Various studies demonstrate the capabilities of NTL, including disaster assessment using different sensors, as well as the corresponding challenges (Zhao et al., 2019; Levin et al., 2020). NTL-based disaster reports have been actively supporting international humanitarian organisations (GEO, 2023).

The NASA Black Marble VNP46 suite—including VNP46A1 (daily, 500 m), VNP46A2 (daily, 500 m), and VNP46A3 (monthly, 15 arc-second)—has been widely applied to disaster assessment through pre- and post-event comparisons. Studies aggregate nighttime light values using means (Lin et al., 2023), sums (Schippers & Botzen, 2023), or customised regional metrics (Zhang et al., 2023), often with temporal smoothing (Lin et al., 2023).

Most applications employ percent-based indicators: Lin et al. (2023) developed Critical Disaster Indicators (CDIs) for outage duration, damage degree, and recovery level; Román et al. (2019) measured percentage recovery, net days without electricity (NDWE), and customer hours of interruption; and Barton-Henry & Wenz (2022) applied monthly percent changes to show incomplete recovery in southern US counties. Similarly, Zhang et al. (2023) combined VNP46A2 and VNP46A3 to derive percentage-based metrics such as average NTL, pre-disaster fluctuation, and relative change ratios.

In contrast, difference-based approaches directly quantify absolute radiance changes between pre- and post-disaster periods. Schippers & Botzen (2023) employed this method to assess Hurricane Katrina's impacts at both pixel and county levels. Principe & Soriano (2022) applied VNP46A2 for STY Yolanda (Haiyan) in the Philippines, using difference-based metrics for spatial analyses and percentage-based metrics for temporal recovery trends. Quizon et al. (2023) also adopted a difference-based framework to characterise power restoration patterns in coastal communities affected by multiple typhoons in the Philippines from 2020 onward.

These studies show how difference- and percent-based metrics reveal disaster impact and recovery dynamics. Building on this, we apply VNP46A3 over 12 years to assess barangay-level impact and recovery from STY Yolanda (Haiyan), integrating both metrics within a unified framework and introducing a prioritisation mechanism to support disaster response and decision-making.

## 3 Materials and Methods

### 3.1 Study Area

The 600 km-diameter STY Yolanda (Haiyan) struck the Philippines in November 2013 as one of the strongest tropical cyclones on record (Fig. 1). The Joint Typhoon Warning Center (2014) reported maximum sustained winds of 195 mph (315 kph), Category 5 on the Saffir–Simpson scale. Locally, the National Disaster Risk Reduction and Management Council (NDRRMC, n.d.) recorded winds of 147 mph (235 kph) and deemed it the most destructive typhoon since 1970, causing approximately 6,300 deaths, 28,688 injuries, 1,062 missing persons, and Php 93 billion damages.

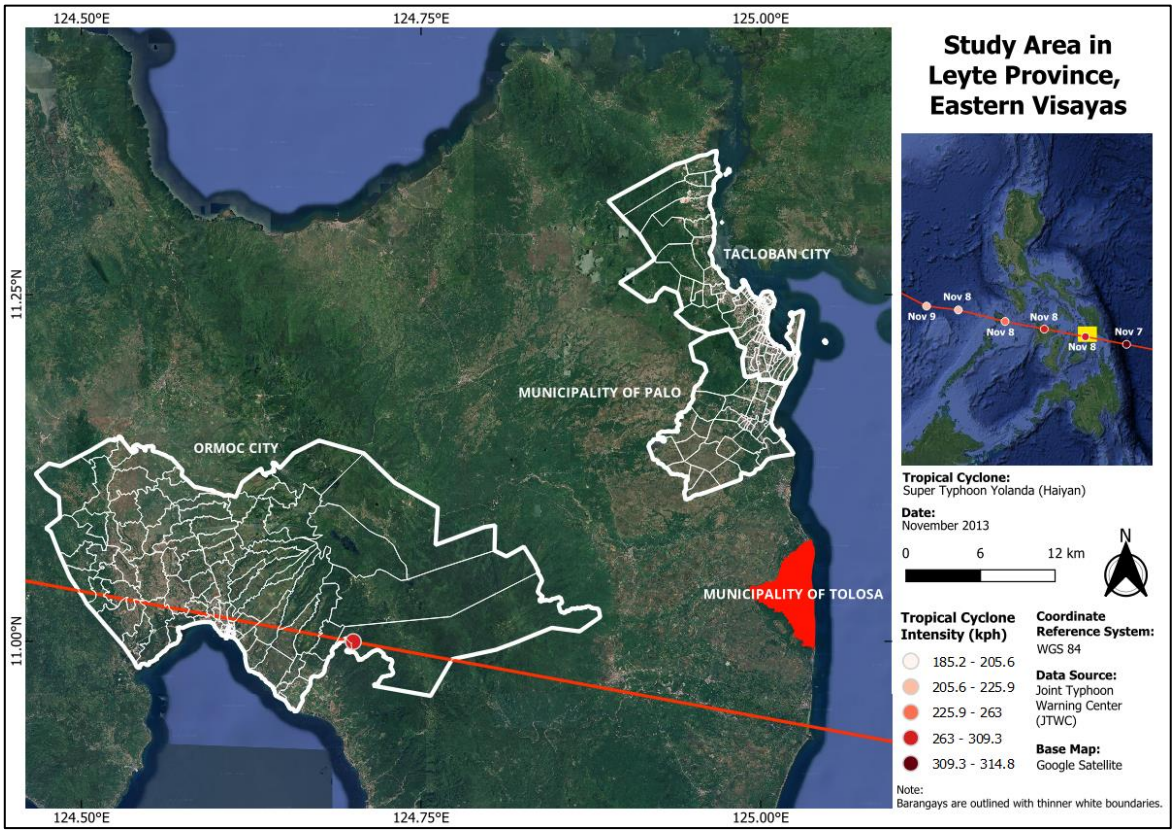


Figure 1: The study area includes parts of Eastern Visayas in Leyte, namely Tacloban City (138 barangays), the Municipality of Palo (33 barangays), and Ormoc City (110 barangays), located near the second landfall in the Municipality of Tolosa.

This study examines three severely affected areas: Tacloban City, Municipality of Palo, and Ormoc City. Tacloban City, a highly urbanised city of 221,174 people, suffered 2,678 deaths (42.51% of all casualties) from an 8.6 m storm surge and flooding, with 58,823 houses damaged (Lagmay et al., 2015; NDRRMC, n.d.). Palo, a third-class municipality of 62,727 residents, experienced 902 deaths from 5.8 m storm surges and flooding, and 14,916 houses were damaged (Mas et al., 2014; NDRRMC, n.d.). Ormoc City, a first-class independent city

of 191,200 people, reported 37 deaths from strong winds and flooding, with 40,681 houses damaged (NDRRMC, n.d.).

### 3.2 Methodology

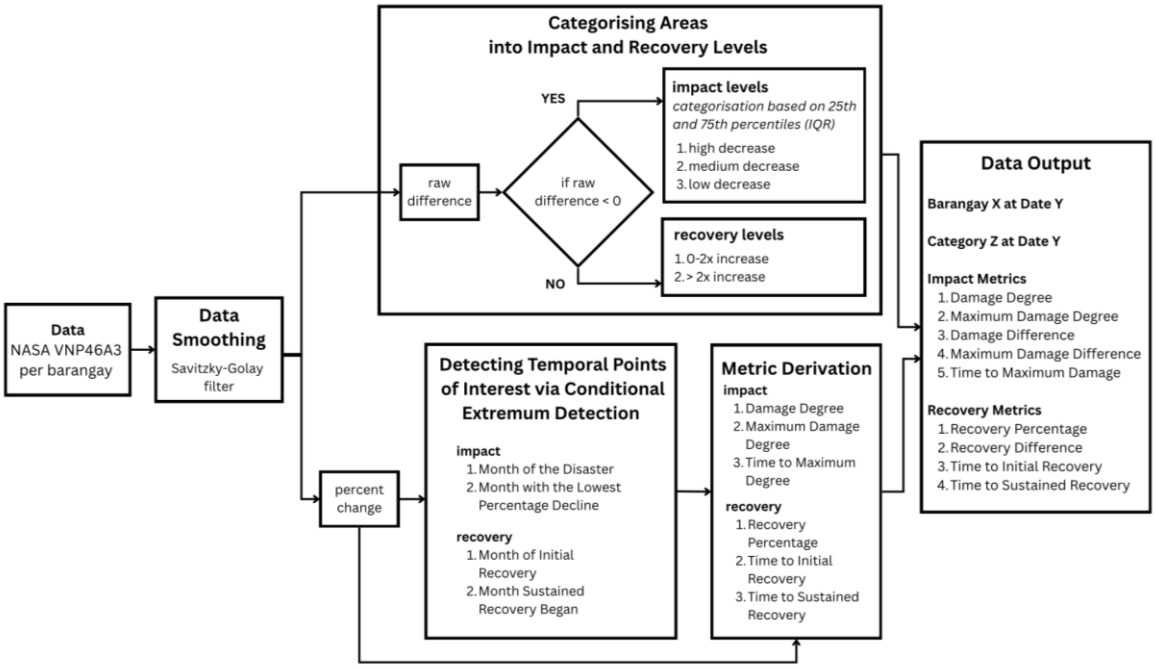


Figure 2: The framework has four main modules: (1) data smoothing, (2) area categorisation by impact and recovery levels, (3) detection of temporal POIs using conditional extremum detection, and (4) metric derivation. These outputs enable various analytical and visualisation tasks.

#### 3.2.1 Dataset

The NASA VNP46A3 VIIRS/NPP Lunar BRDF-Adjusted Nighttime Lights Monthly L3 Global product (May 2013–May 2025) provides monthly, gap-filled, moonlight- and atmosphere-corrected radiance, minimising daily variability to capture stable NTL observations (Wang et al., 2012). We applied zonal statistics using the sum at the barangay level, which, unlike the mean, captures both the intensity and spatial extent of lighting—important for detecting disaster-driven reductions in illumination and lit area. To enable comparisons across areas of varying sizes and baseline brightness, we calculated percent- and difference-based metrics relative to pre-disaster levels.

#### 3.2.2 Data Smoothing

To reduce fluctuations in the VNP46A3 while preserving long-term trends and seasonal patterns, a Savitzky–Golay (S–G) filter (Savitzky & Golay, 1964) was applied. The optimal

window size (N) and polynomial order (p) were determined by jointly minimising the root mean square error (RMSE) of the first derivative (Ahnert & Abel, 2005; Roy, 2020) and the residual variance, expressed as the mean squared error (MSE), of the smoothed series (Kauermann, 2005; see Fig. 3). The derivative RMSE evaluates how well the filter preserves temporal gradients, capturing signal fidelity in rates of change, not just the original signal. It is given by:

$$RMSE_{l'} = \sqrt{\frac{1}{T}\sum_{t=1}^{T}(\hat{l}'_t - l'_t)^2} \quad (1),$$

where $l'_t$ is the first derivative of the original NTL signal at time $t$, $\hat{l}'_t$ is the derivative of the smoothed series, and $T$ is the total number of months. Lower values indicate that the smoothed curve better preserves the local temporal dynamics. In contrast, the residual variance quantifies the degree of short-term fluctuations remaining after filtering, with lower values indicating stronger noise suppression and is given by the following:

$$MSE = \frac{1}{T}\sum_{t=1}^{T}(\hat{l}_x - l_x)^2 \quad (2),$$

This dual-metric approach reflects the classical bias–variance trade-off in time-series smoothing: residual variance captures noise reduction, while derivative RMSE reflects bias in the signal shape. By considering both metrics simultaneously, the S–G filter produced the smoothest possible NTL series without compromising the detection of meaningful temporal dynamics.

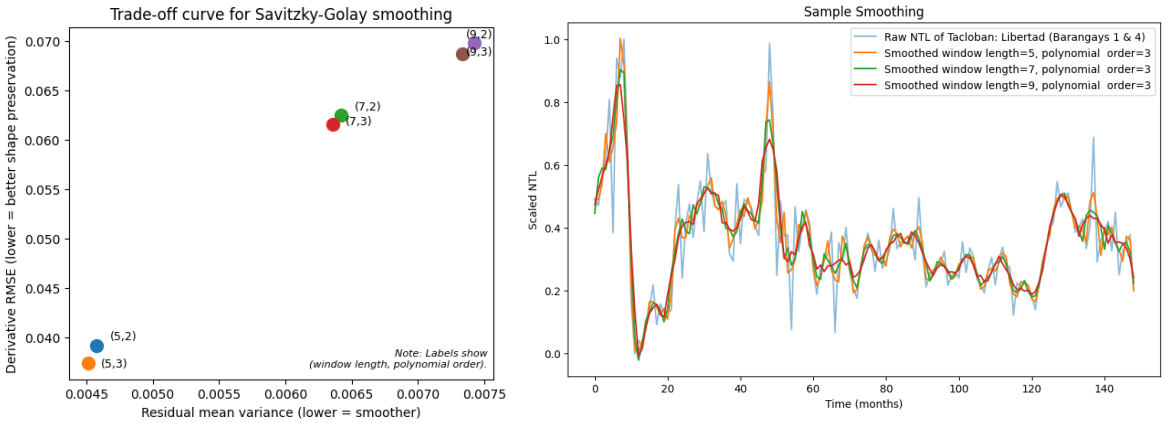


(a) Residual Mean Variance-Derivative RMSE Trade-off Curve

(b) Sample Smoothing of a Barangay Time-series

Figure 3: Trade-off curve showing residual variance and derivative RMSE across S–G parameter choices (window length and polynomial order). The optimal parameters are a window length of 5 and a polynomial order of 3.

### 3.2.3 Categorising Areas into Impact and Recovery Levels

For area categorisation, we use raw difference, as it captures absolute change more reliably than percent-based metrics, which can exaggerate variations with small baselines (e.g., a -90% change does not always indicate severe impact). Percent-based metrics, however, are still employed later to contextualise deviations relative to pre-disaster levels, ensuring both absolute and relative perspectives are considered. Raw difference is given by:

$$Diff_{i,t} = NTL_{post_{i,t}} - NTL_{pre_i} \quad (3),$$

where $NTL_{post_{i,t}}$ is the NTL for an area $i$ and month $t$ after the disaster, and $NTL_{pre_i}$ is the 6-month pre-disaster average radiance (May to October 2013) at a specific area $i$.

We assigned areas with a raw difference $x < 0$ to the impact category. Within this category, values were further classified by the 25th and 75th percentiles: high decrease ($x \leq 25th$), medium decrease ($25th < x < 75th$), and low decrease ($x \geq 75th$). Areas with a raw difference $x \geq 0$ were assigned to the recovery category with two levels defined: 0–2x increase and >2x increase. The >2x threshold was introduced to capture potential population mobility, such as resettlements or expansions.

### 3.2.4 Detecting Temporal POIs via Conditional Extremum Detection

While the raw difference may indicate the same temporal POIs as the percent change, we adopt percent change as the basis for detecting temporal POIs. This is expressed as:

$$\%change_{i,t} = \frac{NTL_{post_{i,t}} - NTL_{pre_i}}{NTL_{pre_i}} x\ 100\% \quad (4),$$

where $i$ refers to an area considering month $t$. A positive value indicates that an area has returned to or exceeded its pre-disaster levels, while a negative value indicates it remains below pre-disaster levels.

Temporal POIs are used to derive the metrics. For impact, the first temporal POI is the disaster month ($t_d$) and the second is the first local minimum, represented as the lowest percentage decline ($t_{lowest}$) given by:

$$t_{lowest} = \min\{t \mid t > t_d,\ \hat{l}_{mins,t} = min_{s>t_d}^{y_s}\} \quad (5),$$

where $\hat{l}_{mins,t}$ is the array of local minima $y$ after the disaster month.

For recovery, the first temporal POI marks the month of initial recovery ($t_{initial}$) which is the first month after $t_d$ in which the percent change becomes non-negative:

$$t_{initial} = \min\{t \mid t > t_d \text{ and } \%change_{i,t} \geq 0\} \quad (6),$$

and the second indicates the month sustained recovery began ($t_{sustained}$), i.e., the first month after $t_d$ when percent change becomes non-negative and remains non-negative until the end of the series T:

$$t_{sustained} = \min\{t \mid t > t_d, \%change_{i,t} \geq 0 \text{ and } \forall \tau \in [t, T], \%change_{i,\tau} \geq 0\} \quad (7),$$

### 3.2.5 Deriving Nighttime Lights Metrics

Using the resulting percent change and key temporal points, we derive a set of NTL metrics to quantify disaster impact and recovery.

For impact, we defined five metrics. Damage Degree ($DD_{i,t}$) represents the percent change at time $t$ after the disaster when it is negative:

$$DD_{i,t} = \{\%change_{i,t} \mid t > t_d \text{ and } \%change_{i,t} < 0\} \quad (8),$$

Maximum Damage Degree ($DD_{max,i}$) corresponds to the percent change at $t_{lowest}$:

$$DD_{max,i} = \{\%change_{i,t} \mid t = t_{lowest}\} \quad (9),$$

Damage Difference ($DDiff_{i,t}$) refers to the raw difference at time $t$ after the disaster when it is negative:

$$DDiff_{i,t} = \{Diff_{i,t} \mid t > t_d \text{ and } Diff_{i,t} < 0\} \quad (10),$$

Maximum Damage Difference ($DDiff_{max,t}$) refers to the raw difference change at $t_{lowest}$:

$$DDiff_{max,i} = \{Diff_{i,t} \mid t = t_{lowest}\} \quad (11),$$

Time to Maximum Damage ($\Delta_{Damage_{max},i}$) is defined as the time index of $t_{lowest}$, with the first element in the series corresponding to $t_d$ at index 0:

$$\Delta_{Damage_{max},i} = index(t_{lowest}) \quad (12),$$

These metrics collectively capture both the magnitude and temporal dynamics of disaster impact across the study area.

For recovery, we computed three metrics to characterise the post-disaster restoration of NTL. Recovery Percentage ($R_{i,t}$) quantifies the overall positive percent change relative to the pre-disaster baseline:

$$R_{i,t} = \{\%change_{i,t} \mid t > t_d \text{ and } \%change_{i,t} \geq 0\} \quad (13),$$

Time to Initial Recovery ($\Delta_{t_{initial},i}$) is defined as the time index of $t_{initial}$ given that $t_d$ is indexed at 0:

$$\Delta_{t_{initial},i} = \text{index}\,(t_{initial}) \quad (14),$$

Time to Sustained Recovery ($\Delta_{t_{sustained},i}$) is defined as the time index of $t_{sustained}$ and represents the elapsed time from the disaster to the point at which recovery stabilizes, indicating a return to a relatively steady NTL level:

$$\Delta_{t_{sustained},i} = \text{index}\,(t_{sustained}) \quad (15),$$

also considering that $t_d$ is indexed at 0. Together, these metrics capture both the magnitude and temporal progression of recovery across the study area.

### 3.2.6 Complementary Information

We compared the resulting patterns with ancillary data, including very high-resolution imagery (Maxar, CNES/Airbus via Google Earth), news articles, NDRRMC situational reports, and other relevant materials. These sources provide context but are incomplete, as power outage reports are typically regional or municipal, with limited barangay-level coverage. Tracking damages is also important, since electricity may be restored while buildings remain unusable. Thus, ancillary sources complement rather than validate results, highlighting the value of nighttime lights for consistent, fine-scale monitoring over time at the barangay level.

## 4 Results and Discussion

### 4.1 Using Percent Change and Raw Difference to Quantify Impact and Recovery

Disaster impact and recovery metrics rely on two metrics: percent change and raw difference in NTL data (Fig. 4). Percent change shows deviations from pre-disaster conditions, highlighting shifts from normal. However, it can exaggerate impacts, particularly in areas with low NTL values. For instance, Barangay 103-A (San Paglaum) had a small raw decrease of -1.3 nW/cm²/sr, yet the percent change was -146.63%. Without context, such figures could suggest a severe impact that does not match observed conditions on the ground.

In contrast, raw difference reflects the absolute change in NTL, more accurately highlighting the areas most affected by the disaster. Heavily impacted locations like Libertad (Barangays 3 & 4) saw a raw decrease of -147.2 nW/cm²/sr, consistent with storm surge, flooding, and damages reported by MapAction and OCHA (2013, 2016). A direct comparison of the two metrics reveals that relying solely on percent change could misleadingly suggest that inland or higher-elevation areas suffered the greatest damage, while raw difference captures the true severity in coastal and flood-prone zones.

To balance both metrics, raw difference categorises areas by absolute changes, while percent change shows relative deviations. For example, Barangay 103-A is classified as low-decrease (-146.63%), and Libertad as high-decrease (-85.11%), reflecting impact severity. Integrating both metrics provides a nuanced view of post-disaster dynamics, prioritising areas with the greatest losses while capturing relative changes for informed planning and equitable recovery.

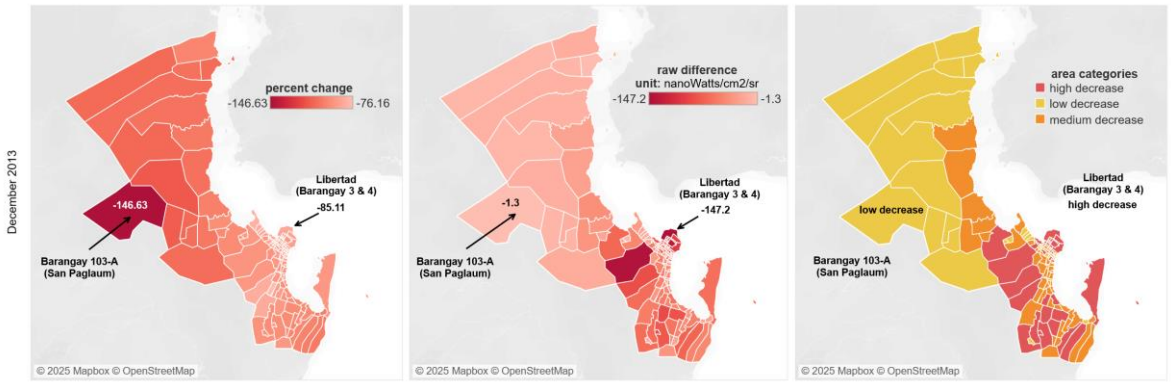


(a) percent change (b) raw difference (c) area categories

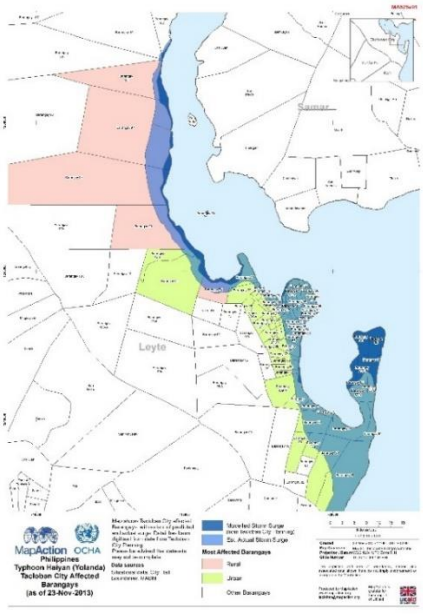


(d) affected barangays with extent of predicted and actual storm surge

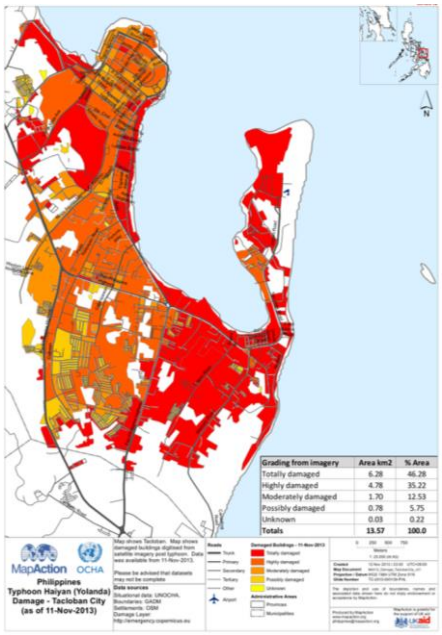


(e) damaged buildings

*Source for (d-e): MapAction & United Nations Office for the Coordination of Humanitarian Affairs (OCHA)*

Figure 4: Tacloban City during its lowest NTL decline (December 2013) (a–c). Spatial variations in NTL are shown as percent change, raw difference, and area classifications of impact. The raw difference and classifications correspond with MapAction & OCHA maps (d–e) of affected barangays, storm surge, and damaged buildings.

### 4.2 Using Nighttime Lights for Tracking Disaster Impact and Recovery, and Prioritising Areas

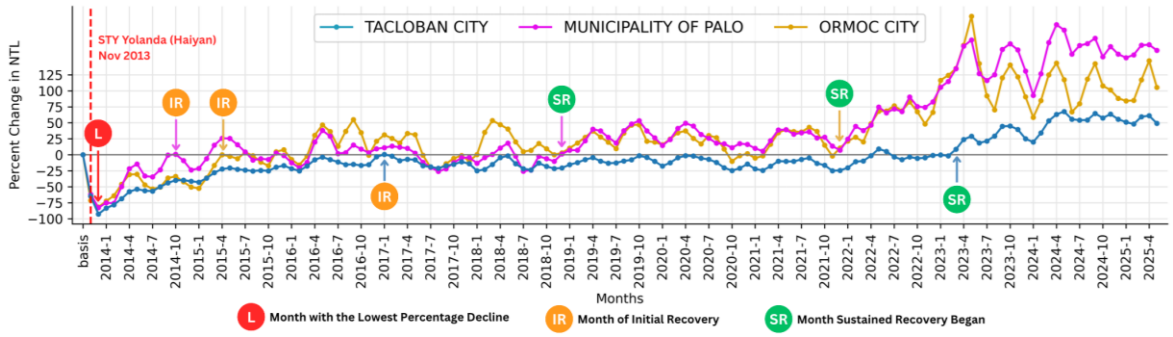


Figure 5: Time-series and temporal POIs at the city and municipal levels

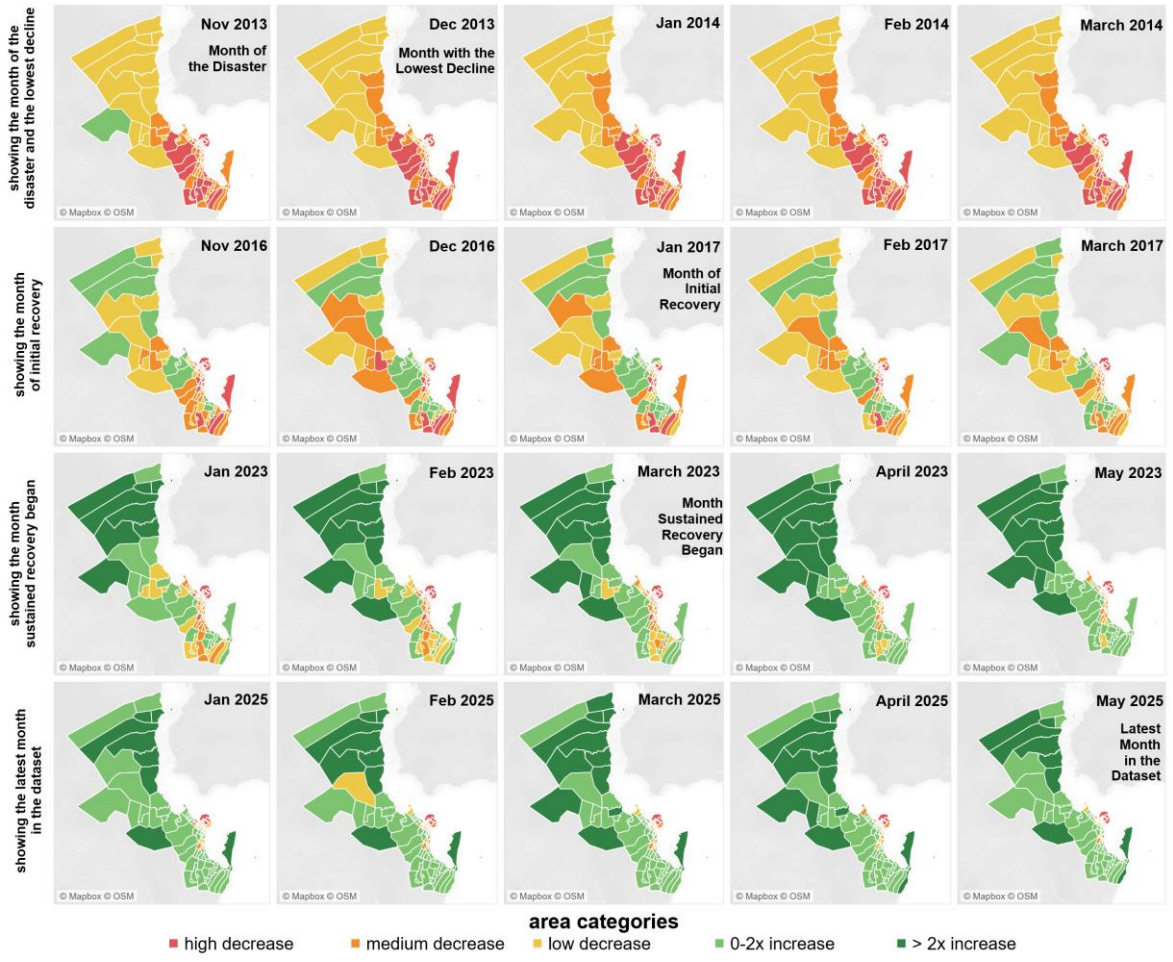


Figure 6: A five-month snapshot timeline showing the impact and recovery progress of Tacloban City through changing area categories across key temporal POIs.

We demonstrate the use of NTL for tracking disaster impact and recovery, alongside area categories, using the identified temporal POIs at the city or municipality level over a five-month period for all three areas (Figs. 5–11). For impact, we consider the period from November 2013 to March 2014, which includes the month of the disaster (November 2013)

and the month with the lowest NTL values (December 2013). For recovery, we focus on periods corresponding to the following temporal POIs: the month of initial recovery, the month when sustained recovery began, and the latest month in the dataset. We found that Fig. 5 aligns with the reports while Fig. 6-11 provides the missing perspectives in the barangay level.

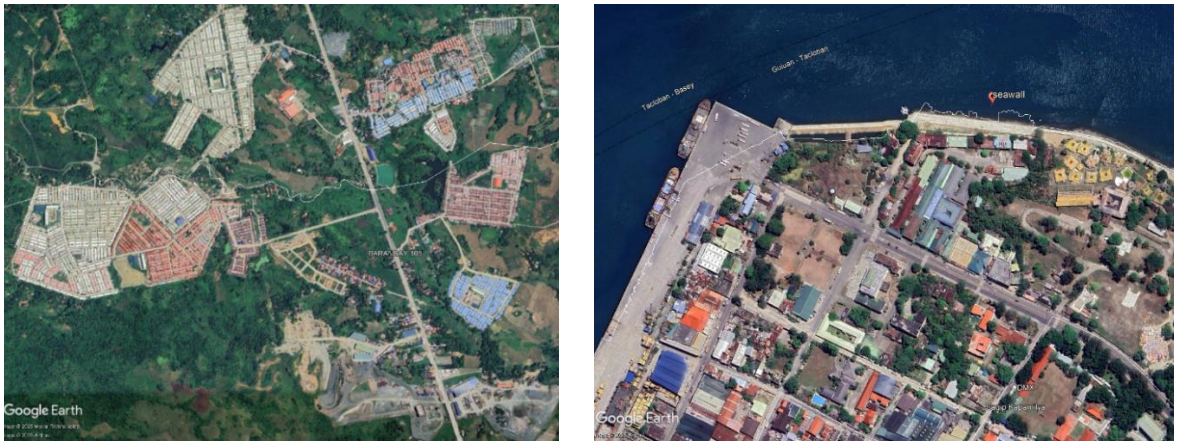


Figure 7: Resettlement sites in Tacloban North, Barangays 105 and 106, captured in March 2025 (left), and the seawall in Libertad, captured in May 2024 (right).

For Tacloban City, the NDRRMC reported province-wide power outages beginning 07 November 2013. Grid-level electricity was fully restored by 24 December 2013, but household access lagged (Regalado, 2013). Tacloban-specific reporting began in January 2014, when 56 of 138 barangays (41%) had electricity, increasing to 115 barangays (83%) by March 2014. Local reports indicated that many households still lacked power, with LEYECO II attributing this to gaps in household access (Gabieta, 2014). Subsequent recovery and population mobility patterns (Fig. 7) show >2x increases largely at resettlement sites (Jopson, 2017), while areas with sustained high decreases correspond to displacement zones influenced by no-build policies and the seawall project (GMA News Online, 2013; Meniano, 2024). As of May 2025, 52 barangays have not yet returned to pre-disaster levels.

Palo was part of the province-wide NDRRMC power outage report on 07 November 2013, though no municipality-specific records existed. Electricity was restored in 17 of 33 barangays by 04 March 2014, with full re-energisation announced on 28 March 2014, while household access lagged (Gabieta, 2014). The impact shown in Fig. 8 aligns with Toda et al. (2016), which identified flood-, landslide-, and storm-surge-prone areas. Recovery, as shown in 0–2x increases between October 2018 and February 2019, was seen mostly below the high decrease zones, mainly near rivers. These areas also saw changes for disaster prevention,

including river dredging in Bangon River (Fig. 9; Department of Public Works and Highways [DPWH], 2023), river walls in Barangay Arado (DPWH, 2020), and nearby resettlement sites (University of the Philippines Centre for Integrative and Development Studies [UP CIDS], 2016). By May 2025, all barangays returned to pre-disaster levels.

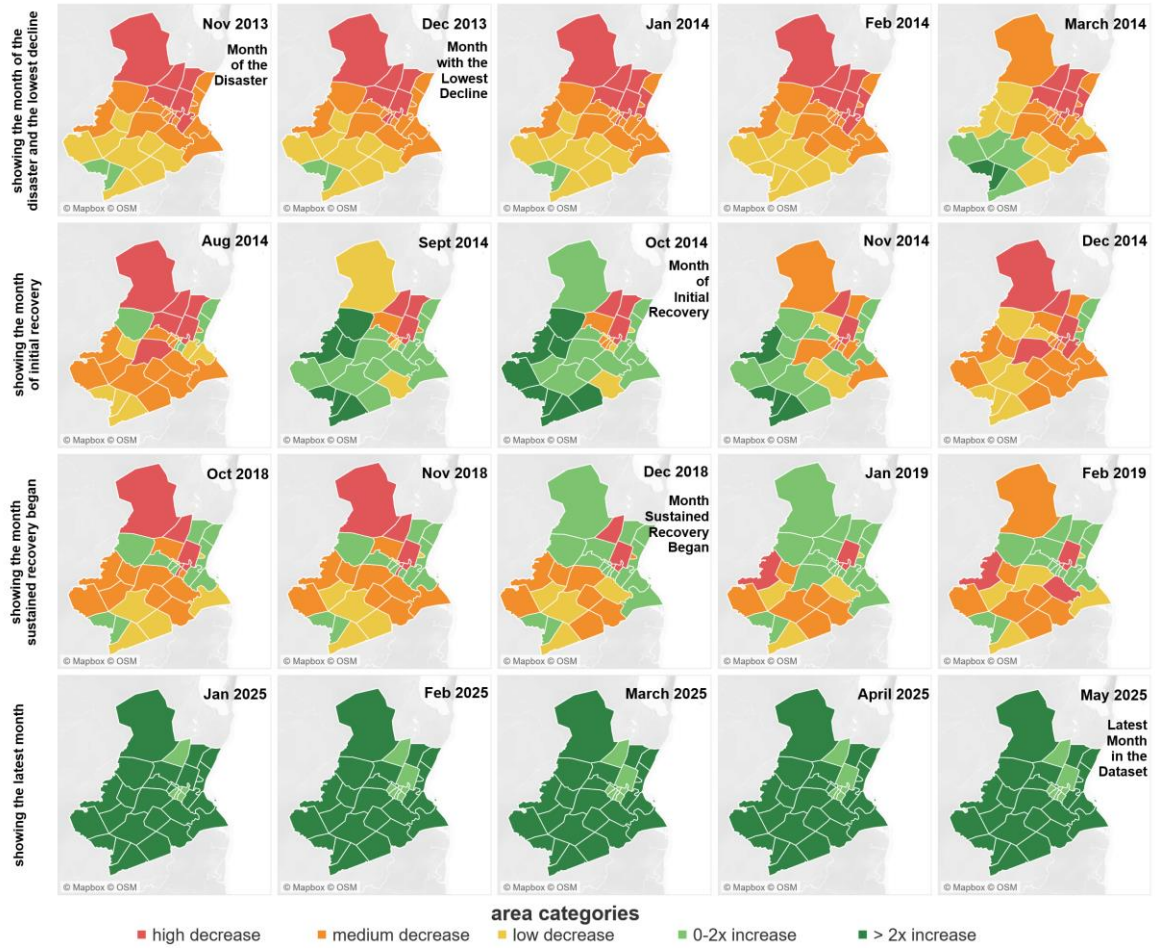


Figure 8: A five-month snapshot timeline showing the impact and recovery progress of the Municipality of Palo through changing area categories across key temporal POIs.


Figure 9: Bangon River near Barangay Guindapunan (the area with highest NTL decrease in Palo) during STY Yolanda (Haiyan) (left) and in the latest available data from March 2025 (right).

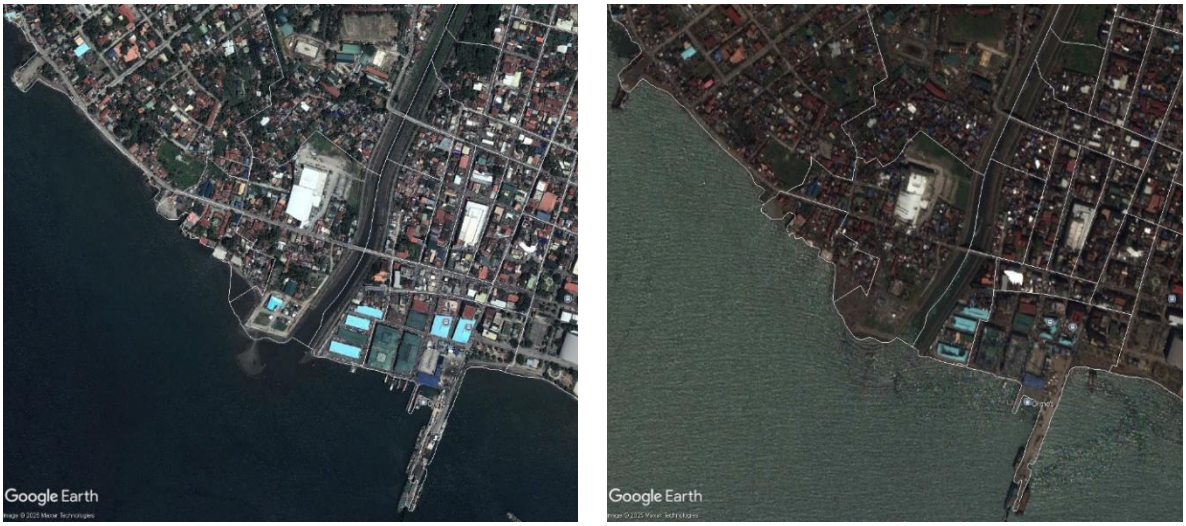


Figure 10: Area near Port of Ormoc City before in August 2013 (left) and during STY Yolanda (Haiyan) (right).

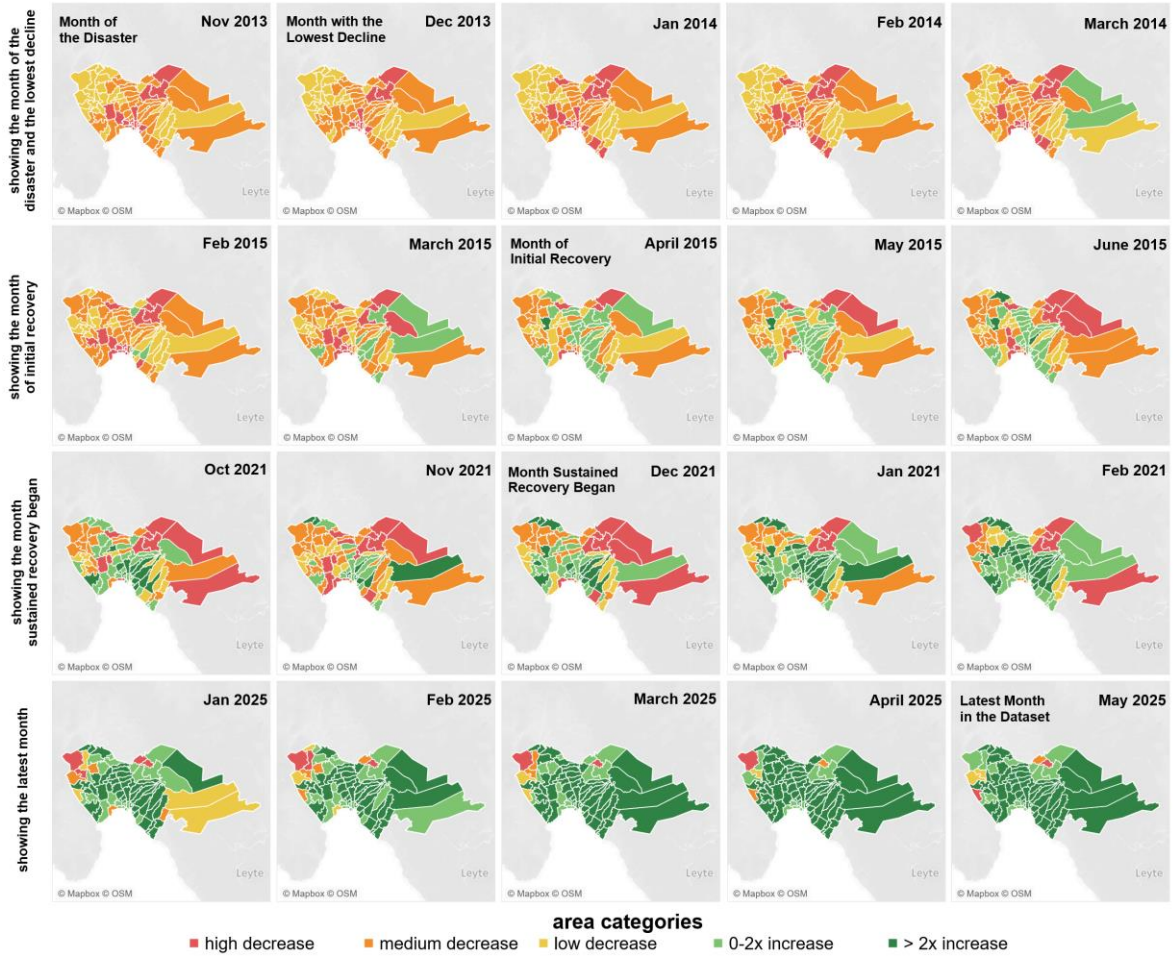


Figure 11: A five-month snapshot timeline showing the impact and recovery progress of Ormoc City through changing area categories across key temporal POIs.

Ormoc City was included in province-wide outage reports starting on 07 November 2013, with the area near the port experiencing severe damages (Fig. 10). Early restorations were

limited to vital structures (NDRRMC, n.d.; Jimenea, 2013). The Unified Leyte Geothermal Complex—including Upper Mahiao, Tongonan, Malitbog, and Mahanagdong—showed a gradual recovery from January 2014, culminating in full restoration by March 2014 (Cruz, 2015), as reflected in the steady NTL increase (Figs. 5 and 11). As of May 2025, five barangays have yet to return to their pre-disaster levels.

### 4.3 Results from the Disaster Metrics

Table 1: Impact metrics for five Tacloban City barangays under the 0–2x increase category, ordered by recovery difference (January 2017).

| | **Brgy. 70** | **Brgy. 79** | **Brgy. 61** | **Brgy. 108** | **Brgy. 43-A** |
|---|---|---|---|---|---|
| **Damage Difference (unit: nW/cm²/sr)** | 0 | 0 | 0 | 0 | 0 |
| **Max Damage Difference (unit: nW/cm²/sr)** | -15.2 | -48.7 | -30.7 | -15.5 | -28.2 |
| **Damage Percentage** | 0 | 0 | 0 | 0 | 0 |
| **Max Damage Percentage** | -82.9 | -97.5 | -95.2 | -98.5 | -86.3 |
| **Date of Max Damage** | 2013-12 | 2013-12 | 2013-12 | 2013-12 | 2013-12 |
| **Time to Max Damage** | 1 | 1 | 1 | 1 | 1 |

Table 2: Recovery metrics for five Tacloban City barangays under the 0–2x increase category, ordered by recovery difference (January 2017).

| | **Brgy. 70** | **Brgy. 79** | **Brgy. 61** | **Brgy. 108** | **Brgy. 43-A** |
|---|---|---|---|---|---|
| **Recovery Difference (unit: nW/cm²/sr)** | 0.1 | 0.3 | 0.4 | 0.7 | 0.9 |
| **Recovery Percentage** | 0.8 | 0.7 | 1.2 | 4.3 | 2.9 |
| **Date of Initial Recovery** | 2015-6 | 2014-8 | 2017-1 | 2016-5 | 2016-12 |
| **Time to Initial Recovery** | 19 | 9 | 38 | 30 | 37 |
| **Date of Sustained Recovery** | 2017-1 | 2017-1 | 2017-1 | 2017-1 | 2016-12 |
| **Time to Sustained Recovery** | 38 | 38 | 38 | 38 | 37 |

Tables 1–2 illustrate the values observed for a specific month, using Tacloban City's initial recovery month of January 2017 as an example. Together with the time-series and maps in Figs. 5–11, they present barangays and their metrics under each area category, here highlighting the 0–2x increase group. Table 1 lists the impact metrics for the five barangays with the lowest recovery difference, showing only historical values such as maximum damage difference and percentage, date of maximum damage, and time to maximum damage. Table 2 combines current recovery metrics (recovery difference and percentage) with previously recorded indicators, including the date and duration of initial recovery and sustained recovery. These historical values provide essential context for interpreting current recovery conditions.

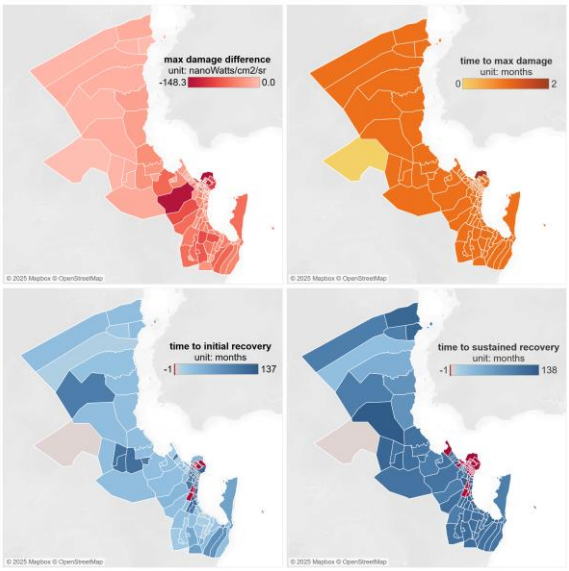


(a) Tacloban City

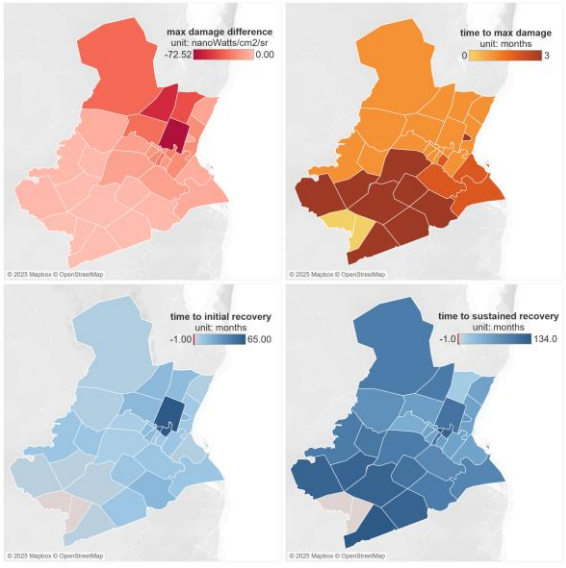


(b) Municipality of Palo

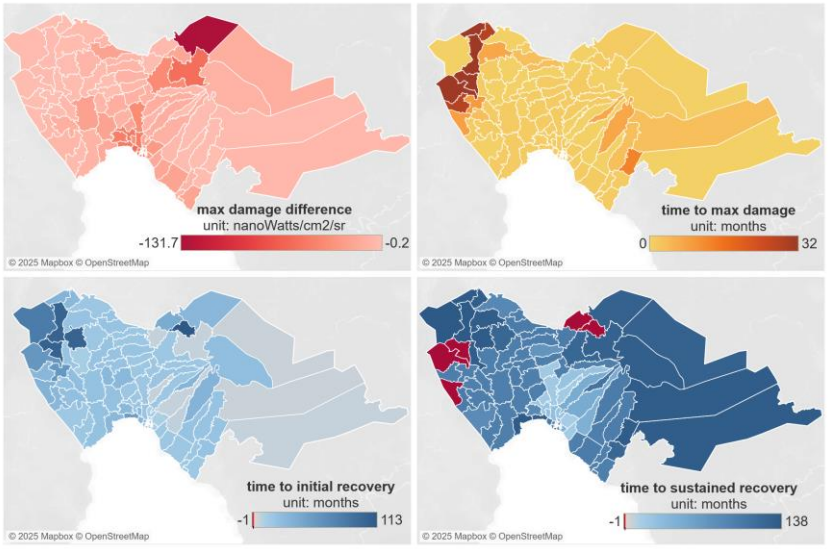


(a) Ormoc City

Figure 12: Metric values for (a) Tacloban City, (b) Municipality of Palo, and (c) Ormoc City, showing variations in maximum damage difference, time to maximum damage, and time to initial and sustained recovery, with -1 indicating areas not yet recovered, by May 2025.

Fig. 12 presents a spatial analysis of damage and recovery metrics, revealing notable differences in disaster impact and resilience across the studied areas. Tacloban experienced the highest intensity of damage, with maximum damage differences reaching -148.3 nW/cm²/sr, and peak damage occurring rapidly within 1–2 months, reflecting the immediate and severe effects of the disaster. In contrast, Ormoc City exhibited a more prolonged damage timeline, with some areas reaching peak damage up to 32 months post-event, indicating ongoing or secondary stressors affecting the region. The Municipality of Palo showed comparatively lower damage intensity and faster recovery rates, with initial recovery occurring within approximately 65 months. These results reveal marked disparities in recovery rates and extent, with Tacloban and Ormoc showing prolonged recovery—even in the initial phase—lasting over 100 months in some areas. The variation in recovery trajectories suggests differences in local resilience, infrastructure robustness, and the effectiveness of relief efforts.

Overall, these findings emphasize the importance of developing tailored recovery strategies that address the unique temporal and spatial dynamics of disaster impacts within each city.

**4.4 Limitations and Future Works**

This study highlights key opportunities for improving both data and methodology. On the data side, the all-angles monthly composite of the VIIRS VNP46A3 nighttime lights product was used to maximise spatial coverage and reduce missing data at the barangay level.

However, further experiments are needed to evaluate sensitivities to different viewing angles. As Wang et al. (2022) noted, results may vary when using all-angles, near-nadir, or off-nadir subsets; comparative analyses could clarify their effects on disaster assessments. Experimenting on the VIIRS VNP46A2 daily product could also complement monthly composites by capturing short-term dynamics at higher temporal resolution. Moreover, the transition to white light-emitting diodes (LEDs)—given the spectral limitations of VIIRS—introduces interpretation challenges for disaster monitoring (Cao & Bai, 2014).

On the methodological side, further work on experimenting with various methods for baseline, filtering, and inclusion of error characterisation can be explored to assess their impact on the resulting time series. Alternative prioritisation schemes—beyond raw differences, percentiles, and thresholds—should also be explored to evaluate their suitability and effectiveness. In addition, integrating complementary geospatial datasets into both tracking and prioritisation frameworks could enhance the comprehensiveness of assessments. Finally, the resulting values from the metrics could be extended to broader analytical applications.

Collectively, these refinements would improve the reliability of NTL data for post-disaster assessment and recovery monitoring, while enabling a more nuanced understanding of temporal and spatial variations at the local level.

## 5 Summary and Conclusions

This study demonstrates a systematic framework for deriving disaster impact and recovery metrics from NTL. By integrating percent- and difference-based indicators with temporal POIs, we provide a flexible system that captures both immediate shocks and long-term recovery trajectories at fine spatial scales. Applied to STY Yolanda (Haiyan), the results confirm severe impacts in coastal barangays, highlight recovery disparities across Tacloban City, Municipality of Palo, and Ormoc City, and reveal persistent recovery gaps more than a decade later.

The framework is highly transferable, enabling application across disasters, regions, and datasets to inform climate resilience, humanitarian action, and policy. Its transparent, reproducible approach for identifying priority areas highlights NTL as a key dataset for scalable, long-term disaster monitoring. Future work should incorporate daily products, additional geospatial layers, and advanced prioritization methods to refine precision and strengthen decision support.

**References**

Ahnert, K., & Abel, M. (2005). Numerical differentiation of experimental data: Local versus global methods. *arXiv*. https://arxiv.org/abs/physics/0510176

Barton-Henry, K., & Wenz, L. (2022). Nighttime Light Data Reveal Lack of Full Recovery After Hurricanes in Southern US. *Environmental Research Letters*, 17(11), 114015.

Cao, C., & Bai, Y. (2014). Quantitative analysis of VIIRS DNB nightlight point source for light power estimation and Stability Monitoring. *Remote Sensing*, 6(12), 11915–11935.

Cruz, E. (2015, February 19). *Yolanda stories from EDC*. Philstar.com. https://www.philstar.com/opinion/2015/02/19/1425342/yolanda-stories-edc

Department of Public Works and Highways (DPWH). (2020, January 17). *DPWH builds P34-M river wall in Palo, Leyte*. DPWH builds P34-M river wall in Palo, Leyte.

Department of Public Works and Highways (DPWH). (2023, January 30). DPWH Undertakes Dredging of Rivers in Eastern Visayas. https://www.dpwh.gov.ph/dpwh/news/29362

Gabieta, J. (2014, April 6). More than 5,000 Tacloban Homes Still Without Power. https://newsinfo.inquirer.net/592100/more-than-5000-tacloban-homes-still-without-power

GMA News Online. (2013, December 13). *Tacloban City Council enacts 40-meters-from-shore building ban*. GMA News Online. https://www.gmanetwork.com/news/topstories/regions/339711/tacloban-city-council-enacts-40-meters-from-shore-building-ban/story/

Group on Earth Observations (GEO). (2023, October 19). GEO Night Light Supports Humanitarian Affairs. https://earthobservations.org/about-us/news/geo-night-light-supports-humanitarian-affairs

Jimenea, L. (2013, November 15). *Power partly restored in Ormoc City*. Philstar.com. https://www.philstar.com/nation/2013/11/25/1260404/power-partly-restored-ormoc-city

Joint Typhoon Warning Center (JTWC). (2013, November). Western North Pacific Ocean Best Track Data. https://www.metoc.navy.mil/jtwc/jtwc.html?western-pacific

Jopson, T. (2017, April 24). *Tacloban North Integrated Development Plan*. Asian Civil Engineering Coordinating Council. https://tc.acecc-world.jsce-int.com/TC21/1704Nepal.files/Presentation_Nepal/08-ted%20Tacloban%20North%20Integrated%20Development%20Plan%204May2016.pdf

Lagmay, A. M., Agaton, R. P., Bahala, M. A., Briones, J. B., Cabacaba, K. M., Caro, C. V., Dasallas, L. L., Gonzalo, L. A., Ladiero, C. N., Lapidez, J. P., Mungcal, M. T., Puno, J. V.,

Ramos, M. M., Santiago, J., Suarez, J. K., & Tablazon, J. P. (2015). Devastating storm surges of Typhoon Haiyan. *International Journal of Disaster Risk Reduction*, 11, 1–12.

Levin, N., Kyba, C. C. M., Zhang, Q., Sánchez de Miguel, A., Román, M. O., Li, X., Portnov, B. A., Molthan, A. L., Jechow, A., Miller, S. D., Wang, Z., Shrestha, R. M., & Elvidge, C. D. (2020). Remote Sensing of Night Lights: A Review and an Outlook for the Future. *Remote Sensing of Environment*, 237, 111443.

Lin, W., Deng, C., Güneralp, B., & Zou, L. (2023). Critical disaster indicators (CDIs): Deriving the duration, damage degree, and recovery level from Nighttime Light Image Time Series. *Remote Sensing*, *15*(23), 5471.

MapAction & United Nations Office for the Coordination of Humanitarian Affairs. (2013, November 12). *Philippines: Typhoon Haiyan (Yolanda) Damage - Tacloban City (as of 11-Nov-2013)*. MapAction and OCHA. https://www.unocha.org/publications/map/philippines/philippines-typhoon-haiyan-yolanda-damage-tacloban-city-11-nov-2013

MapAction & United Nations Office for the Coordination of Humanitarian Affairs. (2016, July 29). *Philippines Typhoon Haiyan (Yolanda) Tacloban City Affected Barangays (as of 23-Nov-2013)*. MapAction and OCHA. https://maps.mapaction.org/dataset/224-3105

Mas, E., Kure, S., Bricker, J. D., Adriano, B., Yi, C., Suppasri, A., & Koshimura, S. (2014). Field survey and damage inspection after the 2013 Typhoon Haiyan in the Philippines. *Journal of Japan Society of Civil Engineers, Ser. B2 (Coastal Engineering)*, *70*(2).

Meniano, S. (2024, November 28). Leyte Storm Surge protection wall 64% complete after 9 years. https://www.pna.gov.ph/articles/1237375

National Disaster Risk Reduction and Management Council (NDRRMC). (n.d.). Situational Report re Effects of Typhoon YOLANDA (HAIYAN). National Disaster Risk Reduction and Management Council. https://ndrrmc.gov.ph/21-disaster-events/1329-situational-report-re-effects-of-typhoon-yolanda-haiyan

Principe, R. L., Jr., & Soriano, M. N. (2022, October 19–21). Revisiting the disaster impact and recovery in the aftermath of Typhoon Yolanda using Black Marble nighttime lights. *Proceedings of the 40th Samahang Pisika ng Pilipinas Physics Conference (Article SPP-2022-3C-04).* Samahang Pisika ng Pilipinas.

Quizon, G. T. M., Principe, R. L., Jr., & Soriano, M. N. (2023, July 19–21). Observing the power restoration trend in Camarines Sur's coastal communities using Black Marble nighttime light data in the 2020 typhoon season. *Proceedings of the 41st Samahang Pisika ng Pilipinas Physics Conference, SPP-2023-PB-07.* Samahang Pisika ng Pilipinas.

Regalado, C. (2023, May 19). Petilla: Power restored in Yolanda-hit areas. https://www.rappler.com/business/46575-power-restored-all-yolanda-hit-areas-petilla-to-keep-his-post/

Román, M. O., Stokes, E. C., Shrestha, R., Wang, Z., Schultz, L., Carlo, E. A., Sun, Q., Bell, J., Molthan, A., Kalb, V., Ji, C., Seto, K. C., McClain, S. N., & Enenkel, M. (2019). Satellite-based assessment of electricity restoration efforts in Puerto Rico after Hurricane Maria. *PLOS ONE*, *14*(6).

Roy, S. (2020). An optimal Savitzky–Golay derivative filter with geophysical applications: An example of self-potential data. *Geophysical Prospecting*, 68(4), 1041–1062.

Savitzky, Abraham., & Golay, M. J. (1964). Smoothing and differentiation of data by simplified least squares procedures. *Analytical Chemistry*, *36*(8), 1627–1639.

Schippers, V., & Botzen, W. (2023). Uncovering the Veil of Night Light Changes in Times of Catastrophe. *Natural Hazards and Earth System Sciences*, 23(1), 179–204.

Toda, L., Orduña, J. R., Lasco, R., & Santos, C. T. (2016). Assessing social vulnerability to climate-related hazards among Haiyan-affected areas in Leyte, Philippines. *Climate, Disaster and Development Journal*, *1*(1), 41–56.

University of the Philippines Center for Integrative and Development Studies (UP CIDS). (2016). Building Back Better: A Democratic Accountability Assessment of Service Delivery After Typhoon Haiyan.

Wang, Z., Shrestha, R. M., Roman, M. O., & Kalb, V. L. (2022). NASA's Black Marble Multiangle Nighttime Lights Temporal Composites. *IEEE Geoscience and Remote Sensing Letters*, *19*, 1–5.

Zhang, D., Huang, H., Roy, N., Roozbahani, M. M., & Frost, J. D. (2023). Black Marble Nighttime Light Data for Disaster Damage Assessment. *Remote Sensing*, 15(17), 4257.

Zhao, M., Zhou, Y., Li, X., Cao, W., He, C., Yu, B., Li, X., Elvidge, C. D., Cheng, W., & Zhou, C. (2019). Applications of Satellite Remote Sensing of Nighttime Light Observations: Advances, Challenges, and Perspectives. *Remote Sensing*, 11(17), 1971.